Unexpected Formation Modes of the First Hard Binary in Core Collapse

Ataru Tanikawa [a,*], Piet Hut [b], & Junichiro Makino [c]

[a] *Center for Computational Science, University of Tsukuba, 1–1–1, Tennodai, Tsukuba, Ibaraki 305–8577, Japan*
[b] *Institute for Advanced Study, Princeton, NJ 08540, USA*
[c] *Interactive Research Center of Science, Graduate School of Science and Engineering Tokyo Institute of Technology, 2–12–1 Ookayama, Meguro, Tokyo 152-8551, Japan*

Abstract

The conventional wisdom for the formation of the first hard binary in core collapse is that three-body interactions of single stars form many soft binaries, most of which are quickly destroyed, but eventually one of them survives. We report on direct N-body simulations to test these ideas, for the first time. We find that both assumptions are often incorrect: 1) quite a few three-body interactions produce a hard binary from scratch; 2) and in many cases there are more than three bodies directly and simultaneously involved in the production of the first binary. The main reason for the discrepancies is that the core of a star cluster, at the first deep collapse, contains typically only five or so stars. Therefore, the homogeneous background assumption, which still would be reasonable for, say, 25 stars, utterly breaks down. There have been some speculations in this direction, but we demonstrate this result here explicitly, for the first time.

1. Introduction

Nowadays, it is recognized that the dynamical evolution of a star cluster is mostly understood as follows (Heggie & Hut, 2003). Two-body relaxation drives core collapse. The core collapse leads to high stellar density region at the cluster center. Owing to the high stellar density, binaries are formed through three-body encounters (Aarseth, 1971; Heggie, 1975; Hut, 1985; Goodman & Hut, 1993). These binaries play important roles for post-collapse evolution, triggering re-expansion of the core, as well as gravothermal oscillations (Bettwieser & Sugimoto, 1983; Makino, 1996).

However, it has not been confirmed whether the binaries are actually formed through three-body encounters, although it has been well investigated how they evolve subsequently, after formation(Spurzem & Aarseth, 1996). Indirect evidence has been gathered indicating that more than three stars might be involved (McMillan, 1988), but no direct observations have been published of the core conditions that lead to the formation of the first binary, in a simulation in which a cluster of single stars undergoes core collapse. In contrast, later hardening of binaries has been described in considerable detail by McMillan et al. (1990) (MHM90).

In this paper, we have followed the dynamical evolution of star clusters by performing *N*-body simulations, in order to catch the moment of binary formation. Upon spotting the first binary, we have then analyzed in detail how this binary formed, with how many other stars involved, and in what kind of step-by-step process.

The structure of this paper is as follows. In section 2, we describe our method for *N*-body simulations and our strategies for catching the moment of binary formation and for analyzing the event. In section 3, we show in detail how the binaries are formed. In section 4, we sum up.

2. Method

We have performed *N*-body simulations of star cluster evolution, up to and slightly past core-collapse. The method for the *N*-body simulations is described in section 2.1. The timescales of binary formation are very much smaller than those of cluster evolution as a whole. This means that the need for high-resolution data around binary formation cannot be simply extended to a full recording of the whole cluster evolution history with the same level of detail. We have to be quite selective in deciding what to store and what to throw out. Our strategy of data compression is described in section 2.2.

* Corresponding author.
  Email address: tanikawa@ccs.tsukuba.ac.jp (Ataru Tanikawa).

2.1. N-body simulation

We have followed the dynamical evolution of five star clusters with equal-mass stars without primordial binaries. Our first three clusters have about a thousand stars, $N = 1k$, another has $N = 4k$, and the last one has $N = 16k$, where $1k = 2^{10} = 1024$. Their initial stellar distributions are given by Plummer's model. Stars in the three clusters with $N = 1k$ are generated with different random seeds, which we label here as seeds 1, 2, and 3.

For the N-body simulations, we have used GORILLA, an N-body simulation code for star clusters (Tanikawa & Fukushige, 2009). This code uses a fourth-order Hermite scheme with individual timesteps (Makino & Aarseth, 1992) for the time integration. The internal orbits of isolated binaries are approximated as Kepler motion. For further details, see TF09.

The accuracy parameter η, and its value at startup, η_s, were set to 0.01 and 0.0025, respectively. We have adopted the standard N-body units, $G = M = r_v = 1$, (Heggie & Mathieu, 1986), where G is the gravitational constant, and M and r_v are respectively the total mass and virial radius of the cluster at the start of the simulation.

We have performed the above N-body simulations on one node of the FIRST cluster at the Center for Computational Sciences in University of Tsukuba (Umemura et al., 2008). Each node of the FIRST cluster is equipped with Blade-GRAPE, a special purpose computer for N-body simulations (Sugimoto et al., 1990; Makino et al., 2003; Makino, 2008).

2.2. Strategy to catch the moment of binary formation

We have caught the moment of binary formation manually, for each simulation. After determining the overall evolution of each cluster by means of an N-body simulation as described in the previous section, we have plotted the time evolution of the number of binaries, shown in figure 1. To be specific, we have disregarded binaries with only modest binding energy, since many of them dissolved again before getting a chance to harden indefinitely. We have chosen our cut-off at $10kT$, where $3/2kT$ is the average stellar kinetic energy in the cluster, i.e. $1kT = 1/(6N)$, at time $t = 0$, at the start of the simulation. The binding energy is expressed as

$$e_b = - \left(\frac{1}{2} \frac{m_1 m_2}{m_1 + m_2} v_{12}^2 - \frac{G m_1 m_2}{r_{12}} \right), \qquad (1)$$

where m_1 and m_2 are the masses of the binary components, and r_{12} and v_{12} are the separation and relative velocity between them. The time in these figures is scaled by the initial half-mass relaxation time. The half-mass relaxation time is defined as

$$t_{rh} = 0.138 \frac{N r_h^{3/2}}{G^{1/2} M^{1/2} \log(0.4N)}, \qquad (2)$$

where r_h is a half-mass radius of a cluster, and $r_h \simeq 0.8$ in the units at $t = 0$.

After thus establishing the exact time of the formation of the first $10kT$ binary, we have done a complete rerun of the same simulation, taking snapshots in much higher time resolution just before and after the moment of binary formation, as illustrated in figure 1. Since the binary is formed in or around the cluster core, it is sufficient to take snapshots only of the core regions. The combination of both temporal and spatial data reduction resulted in orders of magnitude savings in memory needed to store the history of stellar motions around the binary formation events.

We have taken snapshots at very small intervals of $0.01 t_{cr,c}$, only 1% of the instantaneous core crossing time $t_{cr,c}$, given by

$$t_{cr,c} = \frac{r_c}{v_c}, \qquad (3)$$

where r_c is the core radius, and v_c is the stellar velocity dispersion in the core. For relatively large numbers of core stars, we have only included those in our snapshots, but whenever the number of stars in the core fell below a critical value $N_{c,crit}$, we have included the $N_{c,crit}$ nearest stars around the density center. Our choice for $N_{c,crit}$ depends on the number of stars in the simulation: $N_{c,crit} = 40$ ($N = 1k$), 100 ($N = 4k$), and 1000 ($N = 16k$). The density center is defined by the procedure described in Casertano & Hut (1985) (CH85), as modified by MHM90, in which a density around a given star is defined by using the distance to the sixth nearest star.

For typical snapshots, most stars are not synchronized to the time of that snapshot. In those cases, we have derived their positions and velocities through extrapolation, using a predictor given by Taylor series up to the first-order time derivatives of their accelerations, so-called jerk.

We summarize the data of the snapshot files, one for each rerun, in table 1. It is clear that the file size is quite modest; the largest value is about 1 Gbyte, for $N = 16k$, while smaller by almost two orders of magnitude for the other runs. Reasons for the rapid increase of file size with N are the fact that core crossing time decreases for the same selection of time interval in N-body time units, and the increase of the number of stars that we save for larger N values. The fact that the $1k$ runs have a file size that is not much smaller than the $4k$ run stems from the more conservative approach with which we started the former runs, saving data for a longer time span.

3. Results

3.1. Binary formation and core evolution

As is well known, binary formation is closely related to the evolution of a cluster core. When core collapse proceeds, more than two stars interact simultaneously because of the high stellar density in the core. As a result of these

Table 1
Summary for the snapshot file in the final reruns, and $t_{\rm rh,i}$ designates the initial half-mass relaxation time.

N	Seed	Time [$t_{\rm rh,i}$]	Snapshots	File size [byte]
$N = 1k$	1	18.323 - 18.442	14410	19 mega
$N = 1k$	2	20.405 - 20.524	10172	26 mega
$N = 1k$	3	19.490 - 19.542	3087	7.7 mega
$N = 4k$	-	19.8049 - 19.8072	2142	14 mega
$N = 16k$	-	18.5198 - 18.5204	19307	1.2 giga

interactions, a binary is formed. In this section, we investigate the details of core evolution around the time of binary formation.

Figure 2 – 4 show the time evolution of core radii of the clusters, and the moment of first binary formation. The core radii are derived in the same way as CH85 modified by MHM90, in which a density around a given star is defined from the sixth nearest star. In the panels with maximum zoom factor (zoom-2 for $N = 1k$; zoom-4 for $N = 4k$; and zoom-5 for $N = 16k$) time is scaled by the instantaneous value of the core crossing time. We can express this 'co-moving time' τ as

$$\tau = \int \frac{dt}{t_{\rm cr,c}}. \qquad (4)$$

τ effectively presents the accumulation of time on a clock with variable speed, in such a way that each increment in time is scaled by the value of the core crossing time at that particular moment. In this way, the very brief periods of deepest core collapse are guaranteed to be magnified so as to be completely resolved in time. The first binaries are formed during the time interval between the two dashed lines in the panels with maximum zoom factor.

As expected, the time at which the first binaries are formed is comparable for the different runs, when expressed in N-body time units: the first binary in each run is formed between $18 t_{\rm rh,i}$ and $21 t_{\rm rh,i}$. At the time of the formation of the first $10kT$ binary, the core radii are $2 \times 10^{-3} – 2 \times 10^{-2}$ for the $N = 1k$ runs with seed 1 and 2, $1 \times 10^{-2} – 4 \times 10^{-2}$ for the $N = 1k$ run with seed 3, $5 \times 10^{-3} – 1 \times 10^{-2}$ for the $N = 4k$ run, and $1 \times 10^{-4} – 1 \times 10^{-3}$ for the $N = 16k$ run (see the panels with maximum zoom factor in figure 2 – 4).

When inspecting the zoom-1 panels of figures 2, 3, and 4, the core radii around the time pointed at by the arrows take on locally minimal values during intervals of $0.1 t_{\rm rh,i}$ before and after these times. This can be further investigated by following the time evolution of the maximum values of the core radii during fluctuations on smaller timescales than the initial half-mass relaxation time. The maximum values for the core radii, around the times pointed at by the arrows, are 2×10^{-2} for the $1k$ runs, 1×10^{-2} for the $4k$ run, and 2×10^{-3} for the $16k$ run. In contrast, corresponding values at other times during this $0.1 t_{\rm rh,i}$ period are 3×10^{-2} for the $1k$ runs, 2×10^{-2} for the $4k$ run, and 4×10^{-3} for the $16k$ run.

Looking in further detail at the core radii around the time

of binary formation, there is no precise correlation between binary formation and core radii. In fact, core radii at times during which no binary is formed are just about as small as core radii at binary formation time, something that is especially clear in the $4k$ and $16k$ runs (see zoom-3 and zoom-4 of figure 3, and zoom-4 of figure 4, respectively). Core radii are almost constant during $1 \times 10^{-2} t_{\rm rh,i}$ in the case of the $4k$ run (see zoom-3 of figure 3) and $1 \times 10^{-3} t_{\rm rh,i}$ in the case of the $16k$ run (see zoom-4 of figure 4). On the other hand, the binaries are formed during intervals much less than $2.5 \times 10^{-3} t_{\rm rh,i}$ ($4k$) and $5 \times 10^{-5} t_{\rm rh,i}$ ($16k$). The timescale on which core radii small enough to form a binary (about 1×10^{-2} for $4k$ and 1×10^{-3} for $16k$) persist is several times longer than binary formation timescale. We are clearly dealing with events with low probability, even at these high densities, occurring stochastically.

On the way toward binary formation, the core radii sometimes become smaller than any other time by a factor of ten, for example $\tau = -7$ in the $N = 1k$ run with seed 1, $\tau = -7$ in the $N = 1k$ run with seed 2, $\tau = -12$ and -1 in the $N = 16k$ run. These decrease of core radii is not correlated with binary formation. Such decrease of core radii occurs at the other time.

Figure 5 shows the time evolution of the number of stars in the core around the time of binary formation. Note that the numbers of stars in the core around that time fluctuates by roughly a factor or 10, with significant differences between different runs. This in itself already indicates that a homogeneous background density assumption for three-body binary formation breaks down. As we will now see in detail, binaries are indeed formed by processes other than simple three-body encounters.

3.2. Hard Binary Formation Histories

For more than 35 years, the conventional wisdom for the formation of the first hard binary in core collapse has postulated a relatively straightforward picture. While the density of the core increases, near-simultaneous three-body encounters become more and more likely. These can lead to the formation of binaries, where the third star picks up the excess energy, leaving the other two stars bound. Subsequent encounters are most likely to destroy these newly formed soft binaries, but occasionally a soft binary hardens against the odds, and then becomes stable when its binding energy exceeds several kT (Heggie, 1975; Hut, 1983; Goodman & Hut, 1993).

We are now in a position to check this conventional wisdom, using the information we have gathered about orbits of stars and the time evolution of the pair-wise distances between stars in the core.

First, let us have a look at the orbits of stars involving binary formation in figure 6. Apparently, the binary in the $N = 4k$ run, which presents an unusually simple formation case, is formed through an encounter among three single stars. The red, blue, and dark green stars simultaneously

approach each other. Subsequently, the red and blue stars compose of a binary, and the dark green star is ejected from them. This indeed corresponds to the classical picture for binary formation. On the other hand, many stars involve the formation of the binaries in all the other runs. Their orbits are too complicated to determine the mechanism of binary formation from these figures, even though they already suggest a mechanism quite different from the classical picture.

In order to find out more about what is actually happening, we have plotted the time evolution of the pair-wise distances between all stars in the core, during a very small period of time just before binary formation. Figures 7 – 11 show the interactions of stars shown in figure 6 in further detail. Each separate panel shows the distances of one particular star to all other stars in the core. For each curve in a given panel, the color of the curve indicates the identity of the star to which the pair-wise distance is plotted. When some of the curves are intermittent, for example the nearest black curve in the gray panel of figure 8, it is an indication that one or another of the two stars in a pair have temporarily moved outside the cluster core. As described in section 2.2, we have not recorded the data for stars outside the cluster core.

We now describe the evolution histories in detail. We will start with figure 7, where the results for the $N = 1k$ run are given, for seed 1. Just before $\tau = -1.5$, an encounter involving four stars (1, 2, 4, 5) leads directly to the formation of a hard binary (1, 5). A little later, just after $\tau = -1$, that binary dissolves in a complicated dance involving five stars (1, 2, 3, 5, 6), and soon thereafter, around $\tau = -0.5$, a new hard binary (2,3) emerges from this dance. Finally, at $\tau = 0$, a direct three-body exchange leads to the first hard binary (1, 2) with an energy lg $10kT$.

Figure 8 shows the results for the $N = 1k$ run with seed 2. At the start of the interval depicted, there already is a hard binary (8) that was formed earlier; since this binary is only slightly perturbed during this interval, retaining its identity, we have not numbered its two members separately: number 8 indicates both stars as a unit. Also present at the start of the interval is a mildly hard binary (4, 7) which by $\tau = -18$ dissolves during an encounter with three other stars (1, 2, 5). Out of this five-body interaction emerges, soon thereafter around $\tau = -17$, another mildly hard binary (1, 2). This new binary undergoes various perturbations by passing stars, hardening gradually at first. Then, at $\tau = 0$, a close encounter with a single star (3) leads to a sudden increase in binding energy, by a factor of two to three.

Figure 9 shows a similar picture for the $N = 1k$ run with seed 3. Around $\tau = -5$, a three-body encounter (2, 3, 4) leads to the formation of a mildly hard binary (2, 3). A little later, at $\tau = -3.5$, a simultaneous encounter between this binary and two single stars (1 and 5) leads to the formation of a significantly harder binary (1, 2). At $\tau = 0$, a close encounter with a single star (3) leads to a sudden increase in binding energy, by about a factor of two.

Figure 10 shows the $N = 4k$ run. In contrast to the preceding three cases, here hard binary formation is much simpler. At $\tau = 0$ three stars (1, 2, 3) have a simultaneous close encounter, leading directly to the formation of the first hard binary (1, 2) with an energy lg $10kT$.

Figure 11, for the $N = 16k$ run, is again far more complicated. At $\tau = -17$, four single stars (4, 5, 6, 8) meet, producing a mildly hard binary (5, 8). At $\tau = -14$ the binary dissolves in a many-body dance involving several other stars that keep interacting until at $\tau = -9$ a new binary (1, 2) is formed; at the last step in its formation mainly three stars (1, 2, 5) were involved. Finally, at $\tau = 0$, a close encounter with a single star (3) leads to a sudden increase in binding energy, by a factor of two to three.

We conclude from these five cases that direct three-body binary formation is relatively rare. In the one case that we observed, in figure 10, it led to a binary with a binding energy of more than $10kT$, a very different picture than the gradual hardening of a soft binary.

In the other four cases that we studied, the situation was quite a bit more complicated. In all of those cases, there were episodes in which at least four or five stars were simultaneously involved in close encounters that played a role in the formation of the first really hard binary.

4. Summary

In this paper, we have shown that core collapse of star clusters gives rise to the formation of hard binaries via far more complicated processes than have been hitherto considered. Most importantly, the traditional approximation of binary formation through simultaneous encounters of three bodies offers a vastly oversimplified picture of what really happens. Typically, more stars are strongly involved, dynamically, in a complex multi-body dance that in no way can be disentangled to lead to a hierarchy with only three stars in the center.

We have found only one exception, among the five cases studied in great detail. Even in that case, the traditional picture of slow hardening of an initially quite soft binary doesn't apply. Rather, that three-body process of binary formation produced a rather hard binary very quickly, without subsequent hardening encounters with other stars.

We can point to a single reason for the fact that the two core assumptions (3-body encounters, and gradual hardening) of the traditional scenario for hard binary formation turn out to be unrealistic. The main reason for the breakdown of those assumptions is the very small core at the moment of core collapse. What we have found is that, typically, the core at that time contains less than 10 stars, and often only 5 or so stars – so few that a precise measure of the actual number of stars becomes difficult. Given the discrete nature of core stars, the use of continuum properties like density for a population of only 5 stars is obviously rather problematic.

If core bounce would occur at somewhat larger core sizes,

with cores containing twenty to thirty stars or more, the assumptions of three-body encounters and gradual hardening may well have been correct. Following the path breaking analytical investigation of the role of binaries by Heggie (1975) in the seventies, subsequent analytical work in the eighties seems to suggest that core sizes during core bounce remained large enough to ensure Heggie's assumptions. For example, from table 2 of Goodman (1984), equilibrium values of core sizes between $N = 1k$ and $N = 16k$ range between twenty and sixty stars. A more detailed analysis in Goodman (1987) gave rise to his equation (IV.8) suggesting a core size at deep bounce large enough for the core to contain dozens of stars.

Our simulations, in contrast, suggest that deep core collapse causes the number of stars in the core to dip below ten in all cases, independent of the number N of stars for the cluster as a whole. During the final stages before the deepest collapse, the remainder of the cluster is effectively frozen, on the local time scale of the most central regions, and even the order of magnitude of N may become irrelevant. We have demonstrated this for the range $N = 1k$ to $N = 16k$, and we predict a very similar behavior for larger N values, up to $N = 10^6$.

It is an interesting question, why the analytic estimates for the core size at the time of core bounce have overestimated the number of stars in the core $N_{c,min}$ by almost an order of magnitude. Our results indicate $N_{c,min} \sim 5$ while the analytic estimates have predicted results more like $N_{c,min} \sim 30$. One possible reason could be the breakdown of the instantaneous approximation for interactions, used in analytic treatments. With the timescale for formation and subsequent hardening of binaries being comparable to the timescale of core contraction, we may need to extend the analytical approach. We are currently looking into these questions in more detail, continuing the investigations reported here.

Acknowledgment

References

Aarseth,S. 1971, Ap&SS, 13, 324

Bettwieser,K., & Sugimoto,D. 1983, MNRAS, 208, 493

Casertano,S., & Hut,P. 1985, ApJ, 298, 80 (CH85)

Goodman,J. 1984, ApJ, 280, 298

Goodman,J. 1987, ApJ, 313, 576

Goodman,J., & Hut,P. 1993, ApJ, 403, 271

Heggie,D.C. 1975, MNRAS, 173, 729

Heggie,D.C., & Hut,P. 2003, The Gravitational Million-Body Problem: A Multidisciplinary Approach to Star Cluster Dynamics, by Douglas Heggie and Piet Hut. Cambridge University Press, 2003

Heggie,D.C., & Mathieu,R.D. 1986, in Lecture Notes in Physics Vol. 267, ed. P.Hut & S.McMillan (Berlin:Springer-Verlag), 233

Hut,P. 1983, ApJ, 272, 29

Hut,P. 1985, in IAU Symp. 113, Dynamics of Star Clusters, ed. J. Goodman & P. Hut, Dordrecht: Reidel, 231

Makino,J. 1996, ApJ, 471, 796

Makino,J, 2008, in IAU Symp. 246, Dynamical Evolution of Dense Stellar Systems, ed. E. Vesperini, M. Giersz, & A. Sills, Cambridge University Press, 457

Makino,J., & Aarseth,S. 1992, PASJ, 44, 141

Makino,J., Fukushige,T., Koga,M., & Namura,K. 2003, PASJ, 55, 1163

McMillan,S.L.W. 1988, in IAU Symp. 126, The Harlow-Shapley Symposium on Globular Cluster Systems in Galaxies, ed. J. E. Grindlay & A. G. D. Philip, Kluwer Academic Publishers, 669

McMillan,S., Hut,P., & Makino,J. 1990, ApJ, 362, 522 (MHM90)

Spurzem,R., & Aarseth,S. 1996, MNRAS, 282, 195

Sugimoto,D., Chikada,Y., Makino,J., Ito,T., Ebisuzaki,T., & Umemura,M. 1990, Nature, 345, 33

Tanikawa,A., & Fukushige,T. 2009, PASJ, 61, 721 (TF09)

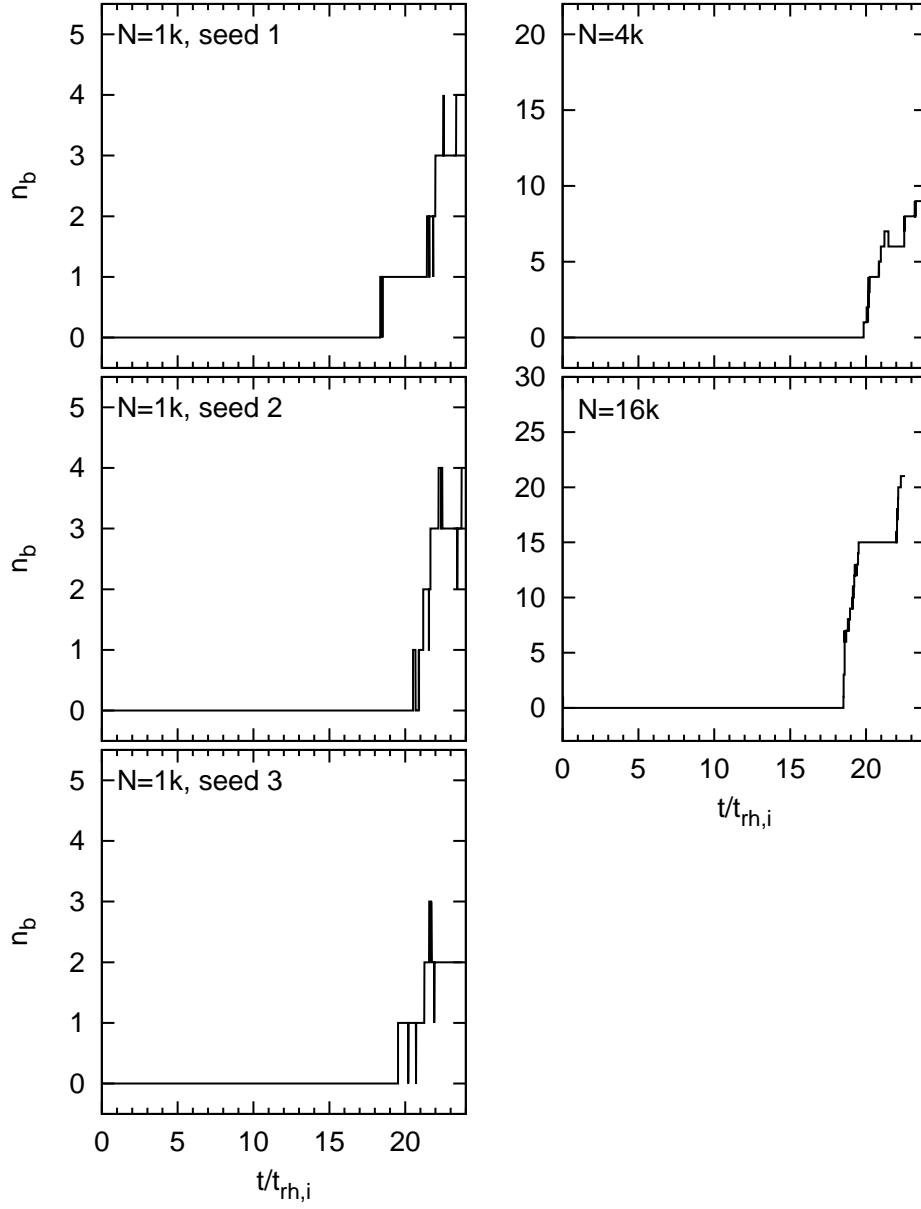Umemura, M., Susa, H., Suwa, T., & Sato, D. 2008, AIP Conference Proceedings, 990, 386

Fig. 1. Time evolution of the number of binaries with more than $10kT$ ($n_{\rm b}$). Time is scaled by initial half-mass relaxation time, defined in equation (2).
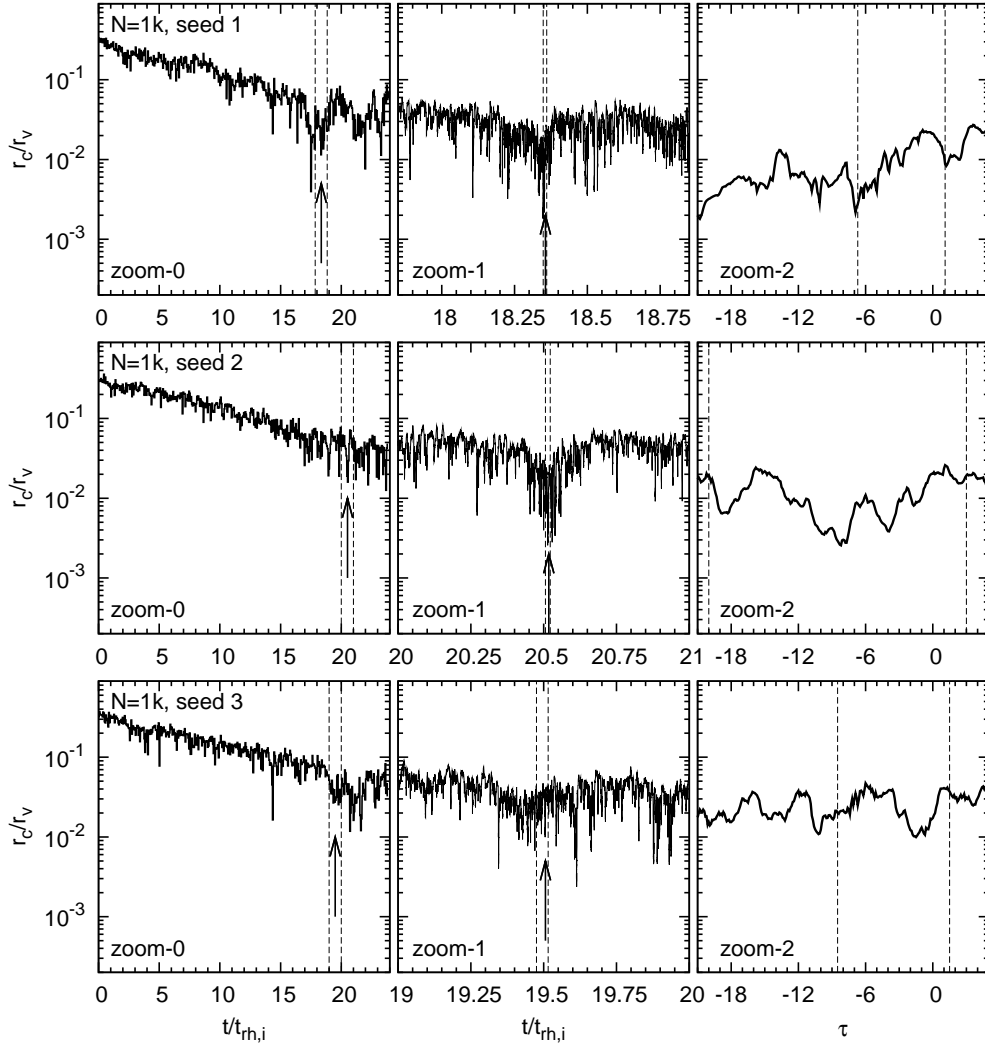
Fig. 2. Time evolution of core radii in the $N = 1k$ runs with seed 1, 2, and 3. The core radii in zoom-0 panels are calculated at each 1 N-body time unit ($5.9 \times 10^{-2} t_{\rm rh}$). Those in the other panels are calculated at each $0.1 t_{\rm cr,c}$. The width of the time in panels zoom-1 is $1 t_{\rm rh,i}$. The range of the time in panel zoom-n is the same as that between two vertical dashed lines in panel zoom-$(n-1)$. The ranges between two vertical dashed lines in panels zoom-2 are the same as those of the time in figure 7, 8, and 9. The arrows and the time $\tau = 0$ show the time when the first binary is formed in each run.
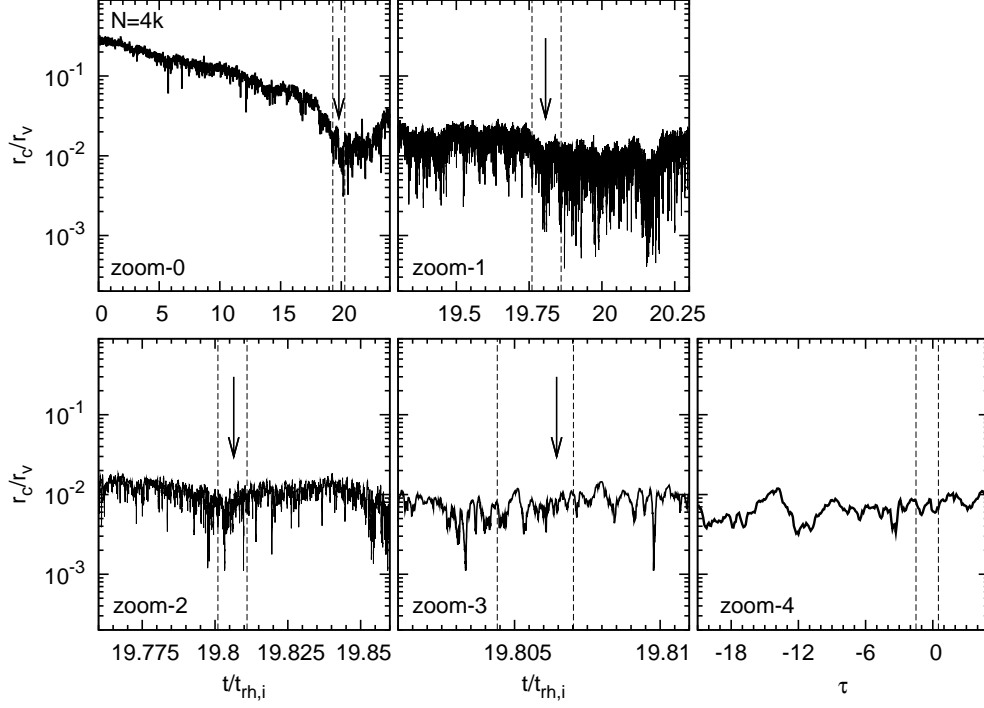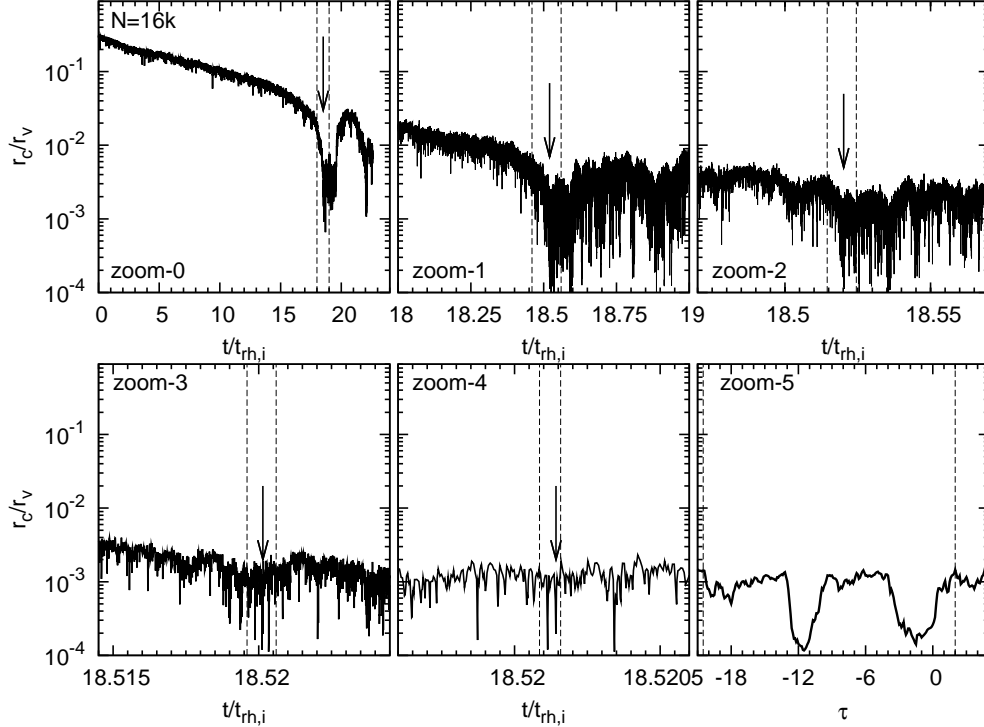
Fig. 3. Time evolution of core radii in the $N = 4k$ run. The core radius in zoom-0 panel is calculated at each 1 N-body time unit $(1.8 \times 10^{-2} t_{\rm rh})$. Those in the other panels are calculated at each $0.1 t_{\rm cr,c}$. The width of the time in panels zoom-1 is $1 t_{\rm rh,i}$. From zoom-1 to zoom-3, the time is zoomed out by ten times step by step. The meanings of the dashed lines are the same as those in figure 2. The range between the two vertical dashed lines in panel zoom-4 is the same as that of the time in figure 10. The arrows and the time $\tau = 0$ show the time when the first binary is formed.

Fig. 4. Time evolution of core radii in the $N = 16k$ run. The arrows and the time $\tau = 0$ show the time when the first binary is formed. The core radius in zoom-0 panel is calculated at each 1 N-body time unit $(5.4 \times 10^{-3} t_{\rm rh})$. Those in panels zoom-1, 2, 3, and 4 are calculated at each $1 t_{\rm cr,c}$, and those in panel zoom-5 at each $0.1 t_{\rm cr,c}$. The width of the time in panels zoom-1 is $1 t_{\rm rh,i}$. From zoom-1 to zoom-4, the time is zoomed out by ten times step by step. The meanings of the dashed lines are the same as those in figure 2. The range between the two vertical dashed lines in panel zoom-4 is the same as that of the time in figure 11.
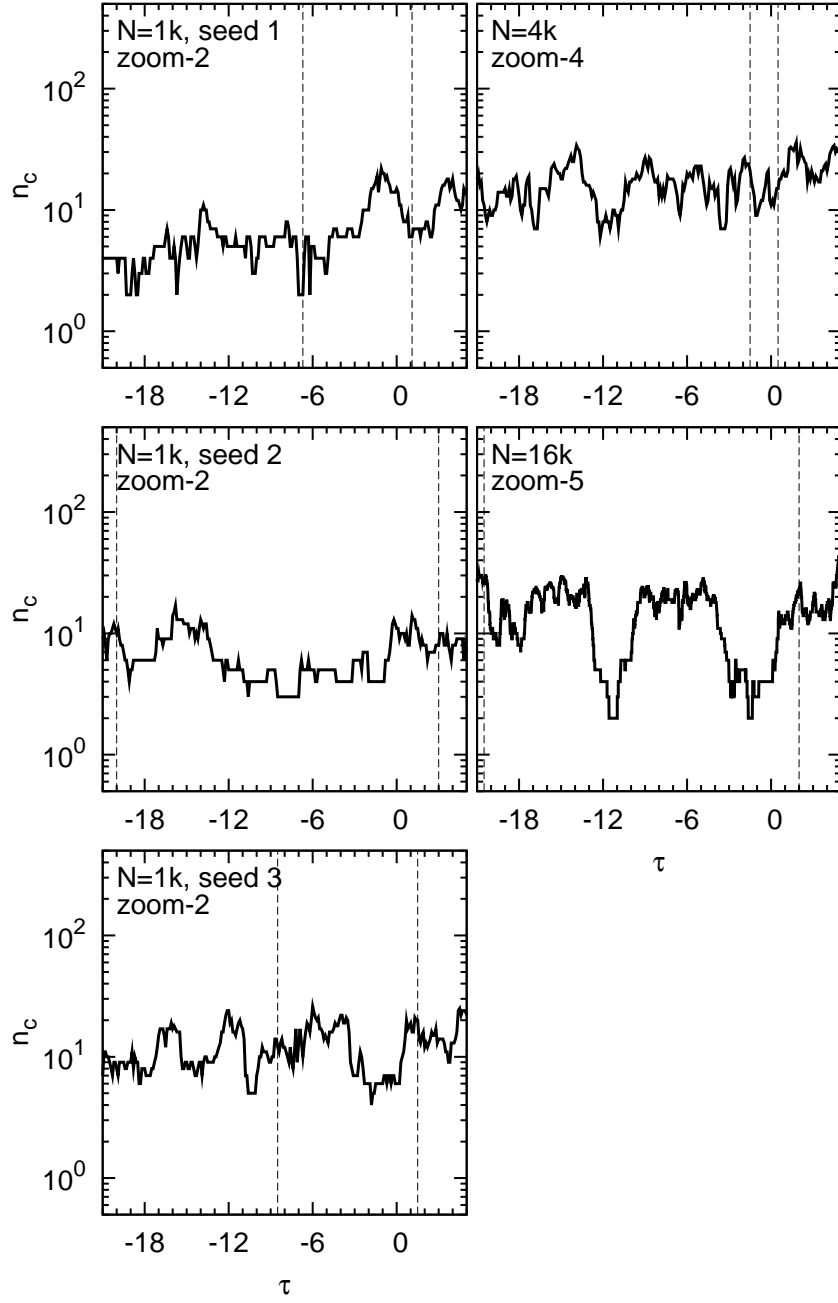
Fig. 5. Time evolution of the number of stars in core at around binary formation in the $N = 1k$ runs with seed 1, 2, and 3, $N = 4k$ run, and $N = 16k$ run.
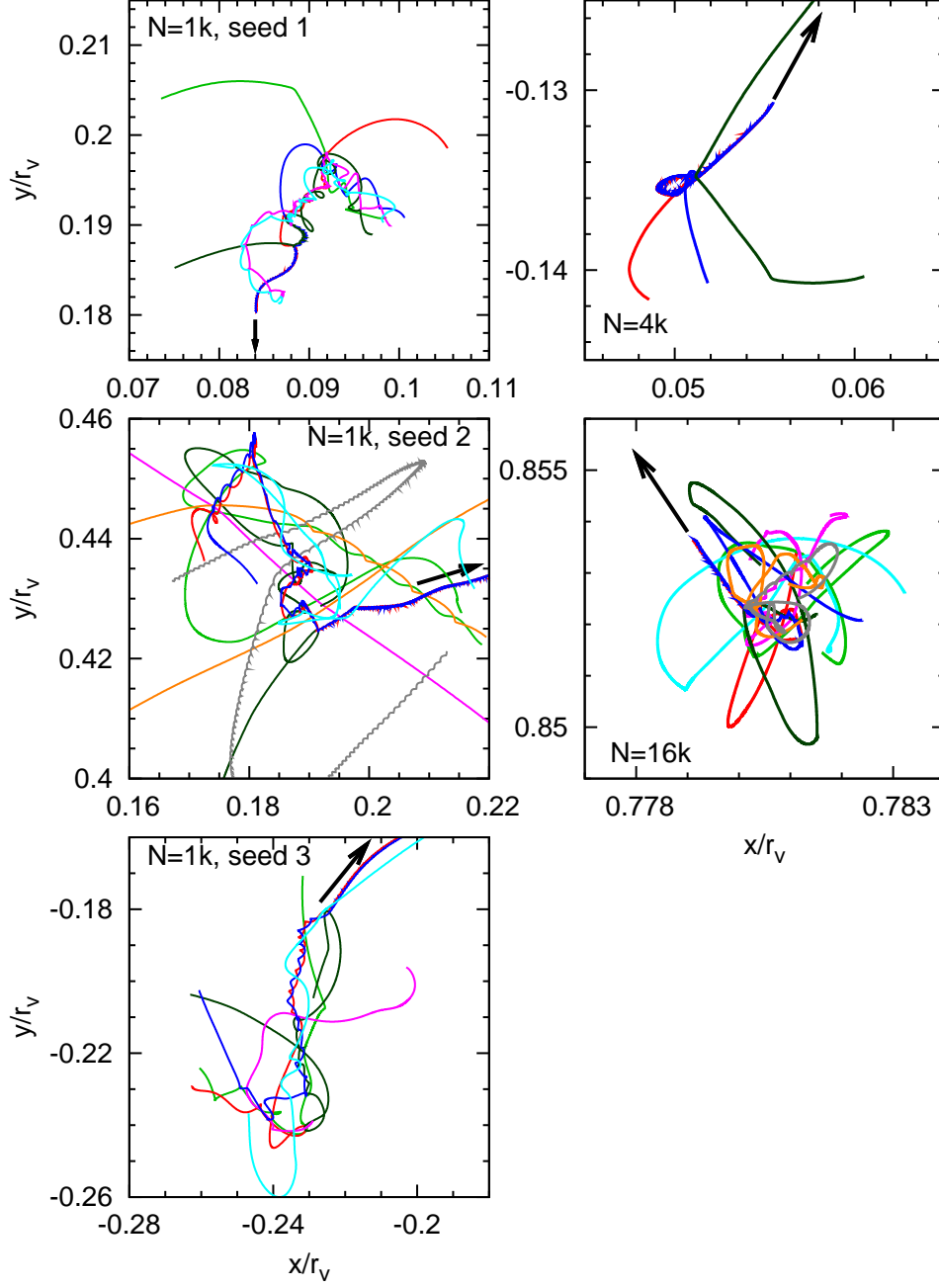
Fig. 6. Orbits of stars involving the binary formation in the $N = 1k$ run with seed 1. The stars whose orbits are drawn by red and blue curves finally become the binary components, and their directions are indicated by black arrows. The time ranges are the same as those in panels zoom-2, 4, and 5 in figure 2, 3, and 4, respectively.
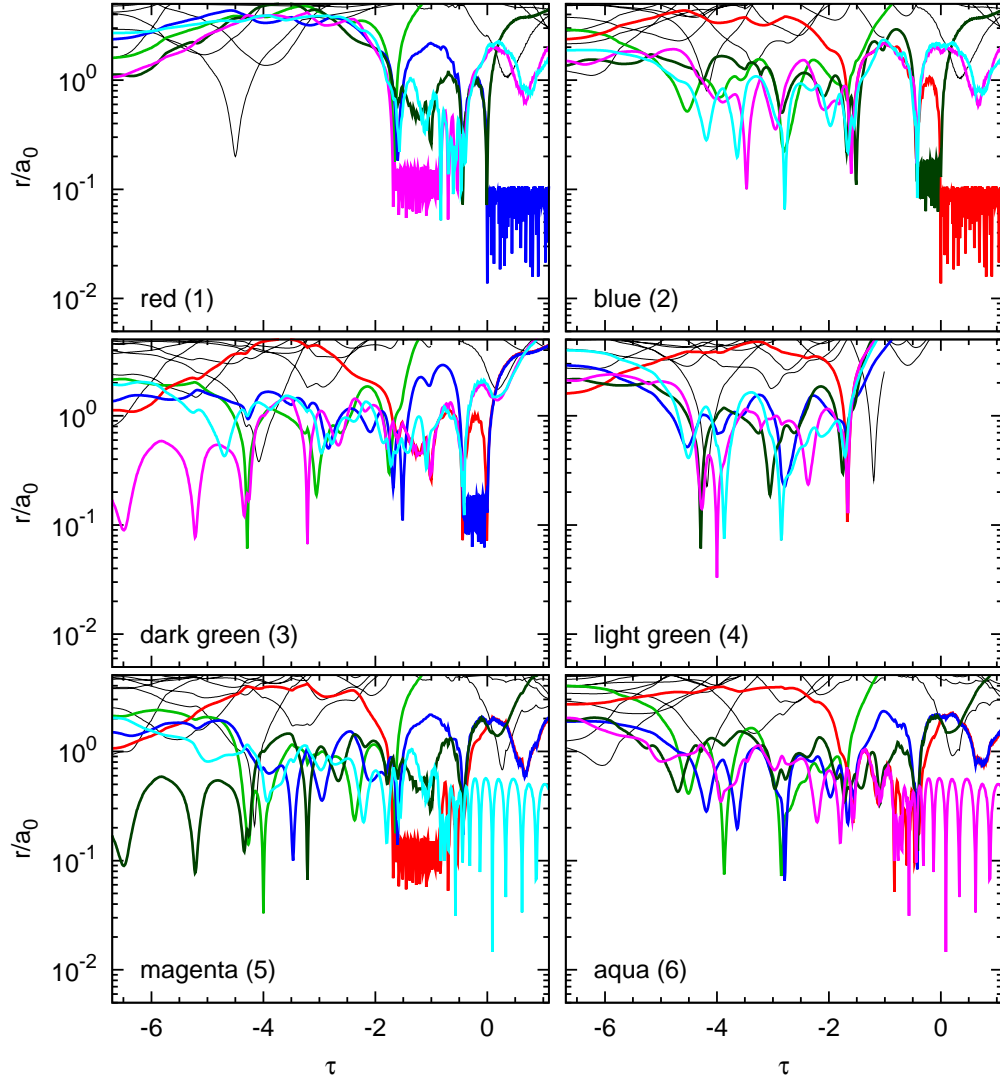
Fig. 7. Time evolution of separations among stars involving binary formation in the $N = 1k$ run with seed 1. The colors are the same as those in figure 6. The black curves indicate stars which do not involve the binary formation. For each star, following the color, the number between parentheses refers to the numbers used in the discussion in section 3.2.
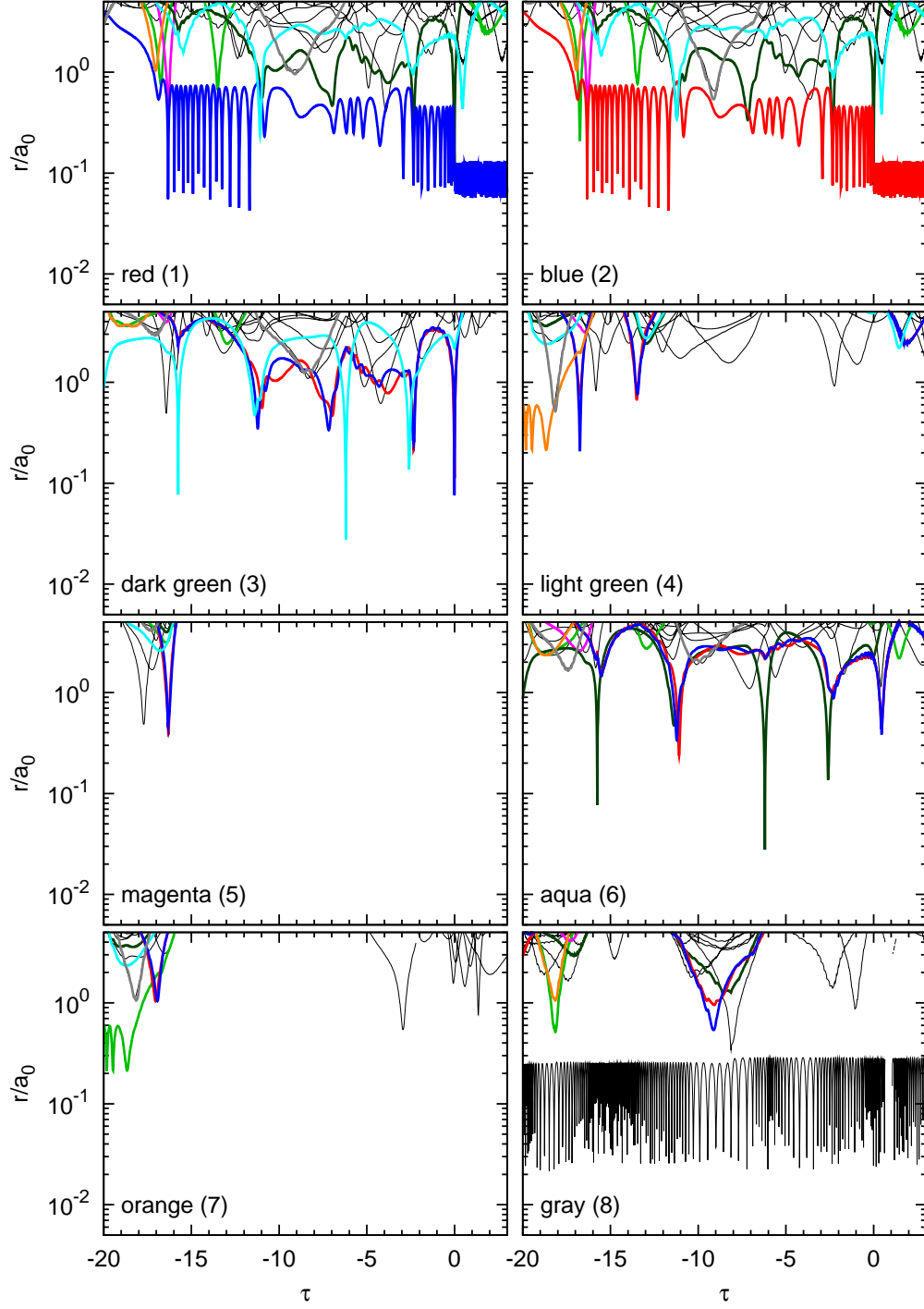
Fig. 8. Time evolution of separations among stars involving binary formation in the $N = 1k$ run with seed 2.
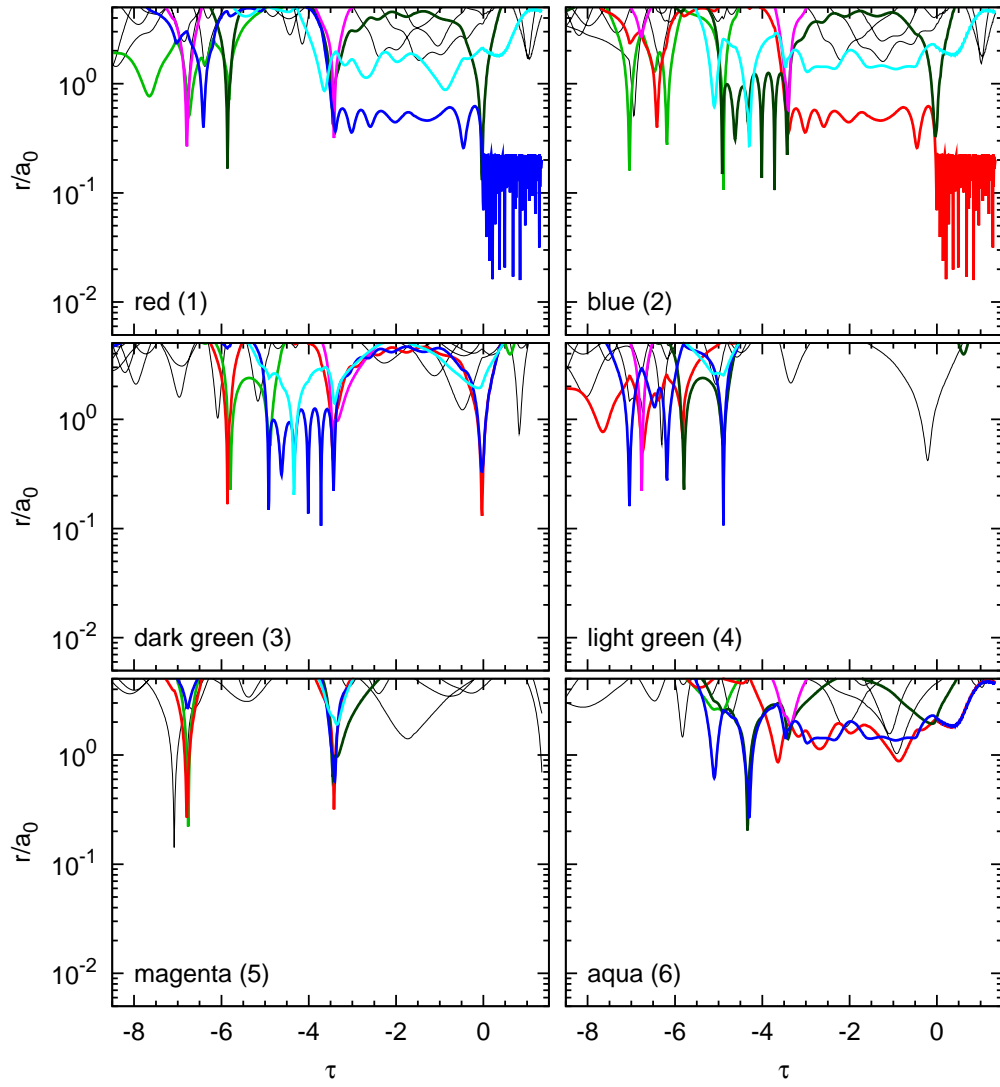
Fig. 9. Time evolution of separations among stars involving binary formation in the $N = 1k$ run with seed 3.
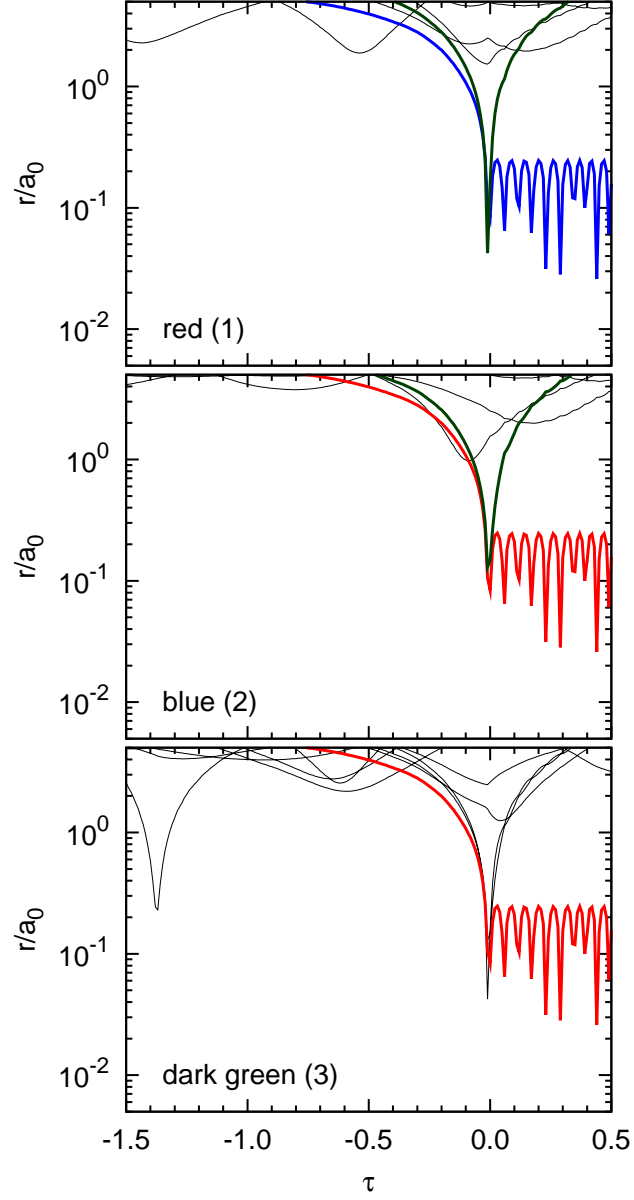
Fig. 10. Time evolution of separations among stars involving binary formation in the $N = 4k$ run.
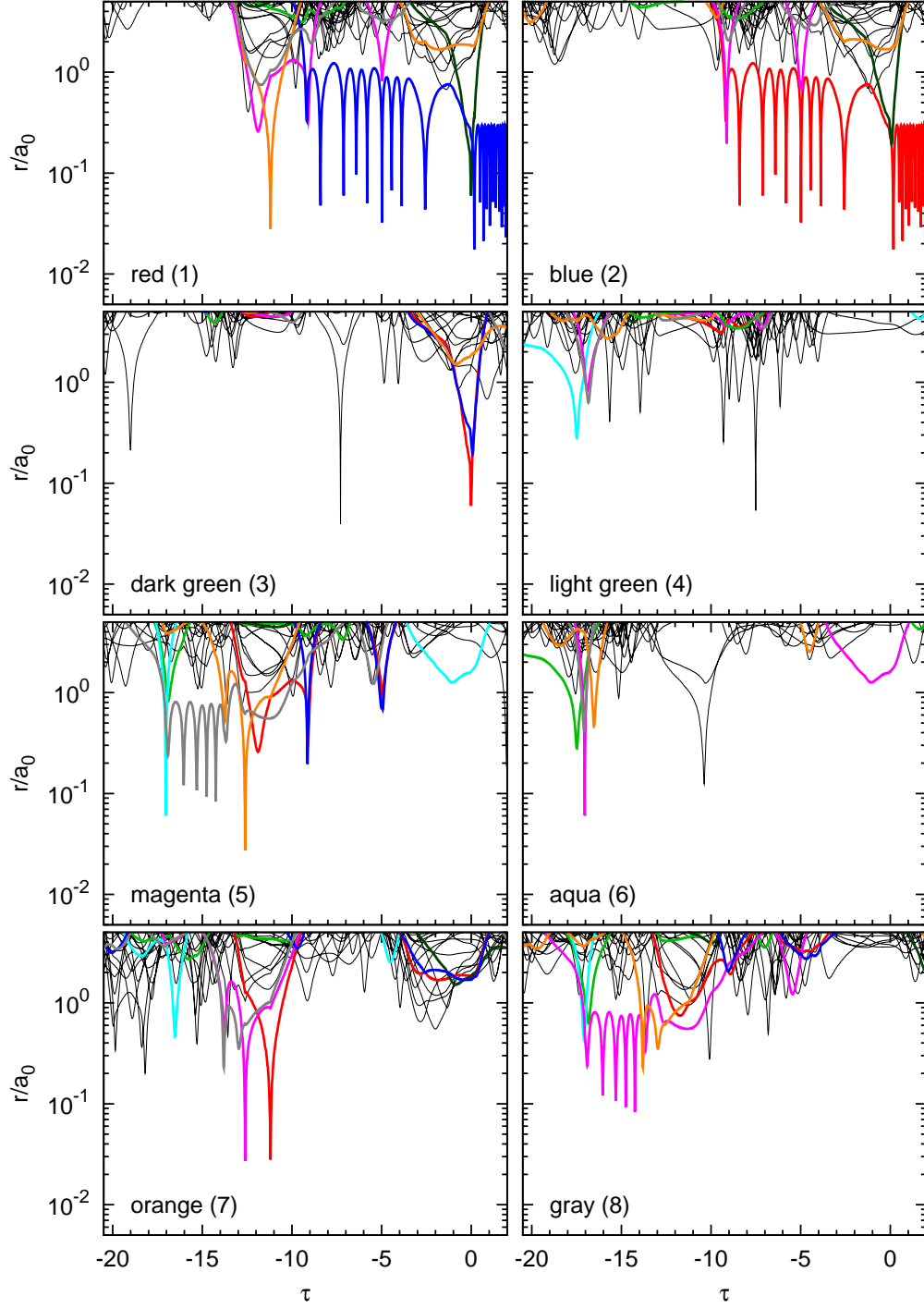
Fig. 11. Time evolution of separations among stars involving binary formation in the $N = 16k$ run.